ACS APPLIED MATERIALS & INTERFACES

Research Article

www.acsami.org

Liquids Analysis with Optofluidic Bragg Microcavities

Manuel Oliva-Ramirez, Lola González-García, Julian Parra-Barranco, Francisco Yubero, Angel Barranco, and Agustín R. González-Elipe*

Nanotechnology on Surfaces Laboratory, Instituto de Ciencia de Materiales de Sevilla (CSIC-USE), Avda. Américo Vespucio 49, E-41092 Sevilla, Spain

Supporting Information

ABSTRACT: Porous Bragg microcavities formed by stacking a series of porous nanocolumnar layers with alternate low (SiO_2) and high (TiO_2) refractive index materials have been prepared by physical vapor deposition at glancing angles (GLAD). By strictly controlling the porosity and refractive index of the individual films, as well as the relative orientation of the nanocolumns from one layer to the next, very porous and nondispersive high optical quality microcavities have been manufactured. These photonic structures have been implemented into responsive devices to characterize liquids, mixtures of liquids, or solutions flowing through them. The large displacements observed in the optical spectral features (Bragg reflector gap and resonant peak) of the photonic structures have been quantitatively correlated by optical modeling with the refractive index of the circulating liquids. Experiments carried out with different glucose and NaCl solutions and mixtures of water plus glycerol illustrate the potentialities of these materials to serve as optofluidic devices to determine the concentration of solutions or the proportion of two phases in a liquid mixture.

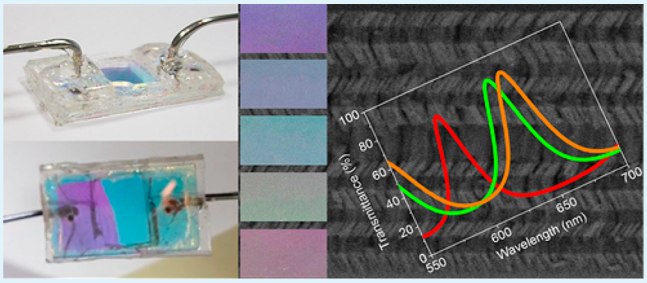

KEYWORDS: *Bragg porous microcavities, optofluidics, TiO_2, SiO_2, GLAD thin films, liquid microsensors*

1. INTRODUCTION

Responsive systems are devices or materials capable of responding automatically in a predictable and reversible way to an external physical or chemical stimulus from the environment.[1] For chemical analysis, such systems may substitute complex analytical instruments and provide simple and reliable procedures for the detection or even the determination of the concentration of a given analyte in a mixture with other components.[2−4] The physical parameters that can be modified by interaction with the environment can be of a different nature and affect the optical, electrical, or even magnetic properties of the material or device. A simple example based on changes in optical parameters refers to the variations produced in the refractive index of porous thin films or multilayer structures when they are exposed to vapors of water or other condensable compounds.[5] Similar changes in the optical response are the basis of the emerging field of optofluidics,[6] where changes in the optical properties of many devices (e.g., wave guides, stacked multilayer or other photonic structures) are reversibly controlled by the incorporation of liquids. Optical lattices with controlled and accessible porosity have been utilized for chemical responsive applications with systems made by the stacking of metal oxide nanoparticles,[7,8] mesostructured thin films,[9,10] clays,[11] macroporous alumina,[12] or porous silicon layers.[5,13,14] In this line, we have recently shown that multilayer structures prepared by physical vapor deposition in the form of one-dimensional photonic crystals (1DPC) may experience a large change in the position of their wide transmission gap when they are infiltrated with liquids.[15] A similar effect has been recently proposed for the identification of solvents by using 1DPC formed by the stacking of polymer layers and titania nanoparticles.[16] A 1DPC, also known as Bragg stack or Bragg reflecting mirror, is a simple photonic structure made by the stacking of successive and alternating layers of two transparent materials with different refractive indices. Due to optical interference processes, these photonic structures produce a reflection of light that extends over a certain range (Bragg gap) of wavelengths producing the impression of a colored mirror. The position and width of the reflecting gap can be tuned by controlling the number of stacking layers, their thickness, and the difference in the refractive index of the two materials.

Planar Bragg microcavities, a modification of 1DPCs, integrate in the center of a Bragg reflector a layer with a different thickness. The incorporation of this layer, considered an optical defect, gives rise to the appearance of a resonance narrow peak in the Bragg gap. Planar Bragg microcavities made of porous silicon prepared by electrochemical methods have been proposed for sensing vapors[5,13,14] or for the development of advanced biosensing tests.[17−19] The integration of a nonplanar Bragg microcavity fabricated by electron-beam lithography and reactive ion etching techniques into a

Received: May 6, 2013
Accepted: June 19, 2013
Published: June 19, 2013

   dx.doi.org/10.1021/am401685r | ACS Appl. Mater. Interfaces 2013, 5, 6743−6750

microfluid device for optofluidic applications has been reported recently.[20]

In the present work, we report the fabrication of planar Bragg microcavities by stacking successive layers of two transparent and porous oxides prepared by e-beam evaporation in a glancing angle configuration (GLAD).[15] This geometrical configuration renders films formed by tilted nanocolumns with a considerable amount of void space in the form of meso- and micropores (i.e., pores larger or smaller than 2 nm according to IUPAC[21]). A full account of the pores and other characteristics of this type of thin films can be found in recent publications.[22−24] GLAD thin films have also been deposited to modify the channel walls of microfluidic devices to facilitate the circulation of liquids[25] or to provide high surface area substrates to increase the anchoring capacity of active molecules used for molecular recognition.[26] However, no essays have been reported about the direct use of GLAD thin film structures as microfluidic components, a fact that is likely related to the difficulty of accurately controlling the porosity and optical properties of both the individual GLAD thin films and the collective response of the final microcavities. A first objective of the present work is to prove that the optical properties of porous GLAD microcavities can be accurately controlled without incurring light dispersion effects very common when dealing with other types of porous materials. Subsequently, we show that these porous structures can be integrated in the form of planar microfluidic components through which liquids can circulate easily. Using this configuration, we show that planar Bragg microcavities, made by stacking several porous TiO_2 and SiO_2 GLAD thin films, can be used as efficient optofluidic responsive systems for measuring the solute concentrations of liquid solutions or for the analysis of liquid mixtures. Case examples of the response of these devices and the modeling of their optical response by using a conventional interference optical model[27] complete the present work.

2. EXPERIMENTAL AND METHODS

Uniform, mechanically stable, and highly porous Bragg microcavity structures made of alternated layers of TiO_2 and SiO_2 with a thicker SiO_2 central layer have been prepared by glancing angle physical vapor deposition (GLAD). Porous layers were successively e-beam evaporated on glass plates of 1.2 × 2.5 cm^2 at glancing zenithal angles of 70° and 80° (α). SiO_2 and TiO_2 were used as target materials while an oxygen pressure of approximately 10^{-4} Torr was kept in the chamber during the evaporation to ensure the complete oxidation of the evaporated oxides (i.e., to get TiO_2 and SiO_2 stoichiometries) and hence their full transparency (TiO_x or SiO_x with $x < 2$ are colored). The GLAD geometry produces films with a characteristic tilted columnar morphology which is controlled by shadowing effects.[22] The results reported here refer to structures consisting of 2 × 7 individual layers of approximately 85 nm thickness, plus one SiO_2 middle layer of approximately 180 nm thickness. The thickness of each individual layer was controlled by means of a quartz crystal monitor calibrated with the actual thickness of layers determined by cross section SEM.

Preparations were carried out by azimuthally turning the substrate 90° when changing the evaporation from one oxide to the other. Turning azimuthally the substrate between two layers is required to avoid the dispersion of light, an effect that has been previously addressed in a work on porous 1DPC used to prepare dye sensitized solar cells.[28]

The stacked layers deposited on a glass plate were sandwiched with another glass plate provided with two holes where liquid tubes acting as inlet/outlet channels of the fluids were fixed. The perimeter of the ensemble was sealed with PDMS to ensure the tightness of the system. A scheme of the system is presented in Figure 1, together with a view of a real device fabricated in the course of this work. In this device, the space between the two glass plates is completely filled with the microcavity structure, and the fluids flow by passing through the pores of the films by just applying a small pressure difference between the inlet and outlet tubes. It could also be realized that liquids with low viscosity and surface tension can pass spontaneously driven by capillarity forces. This configuration ensures that pores are completely filled with the liquid and that an easy and immediate replacement of one liquid by another is possible by just changing an external reservoir connected to the device. Another important clue, proved by simulating[27] the optical response of the system, was that no empty space is left between the stacked microcavity and the glass cover plate.

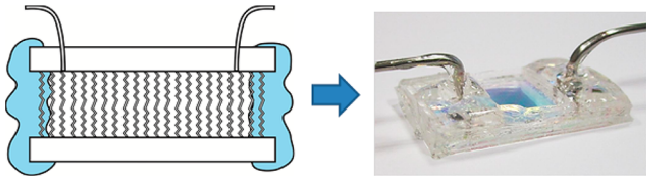

Figure 1. (left) Cross section scheme and (right) image of an optofluidic device based on a Bragg microcavity prepared by GLAD. Note that the different parts in the scheme are not plotted on the same scale.

Cross section SEM micrographs were obtained in a Hitachi S4800 field emission microscope for samples deposited on a silicon wafer that were cleaved for cross-section analysis.

UV−vis transmission spectra were recorded in normal and off-normal configurations with a Cary 100 instrument. For recording at off-normal angles, the optofluidic device was turned with respect to the light beam by using a goniometer provided with a holding piece.

Simulation of the optical response of the Bragg microcavities was done by optimized fitting of the transmittance spectra using a homemade code based on the transfer-matrix approach.[27] The effect of the porosity was incorporated within the Maxwell−Garnett effective medium approximation. Typical Cauchy dispersion was considered for the wavelength dependence of the refractive index of the films in the microcavities. The refractive index and the thicknesses of the porous SiO_2 and TiO_2 layers filled with different liquids in the two seven-layer Bragg reflectors and the SiO_2 defect layer were obtained through the fitting procedure. Close attention was paid to correctly describing the optical gap and the position of the resonant peak in the microcavity.

3. RESULTS AND DISCUSSION

3.1. Microstructure and Optical Properties of Bragg Microcavities Prepared by GLAD. Figure 2 shows a cross-section SEM micrograph of a GLAD porous Bragg microcavity integrated by two Bragg reflectors made of seven stacked layers of SiO_2 and TiO_2 sandwiching a thicker SiO_2 layer as indicated by the diagram of the figure. The thickness of the SiO_2 and TiO_2 stacked layers was about 80 nm, while that of the SiO_2 defect was around 180 nm. An accurate control of the optical properties of the microcavity was possible by changing these thickness dimensions. The whole structure was prepared by GLAD at a fixed zenithal angle of α = 70° by turning the substrate 90° from one layer to the next. This azimuthal rotation was essential to decreasing the dispersion of light at low wavelengths, a common phenomenon found for relatively thick GLAD oxide films. Similar structures were grown by performing the evaporation at a zenithal angle of 80°. The SEM micrograph of an 80° microcavity and a scheme of the relative orientation of the nanocolumns in each layer of the structure resulting from the 90° azimuthal rotation are reported as Supporting Information (S1).

It is worth stressing that compared with conventional silicon porous Bragg microcavities prepared by controlled electrochemical oxidation followed by annealing at high temper-

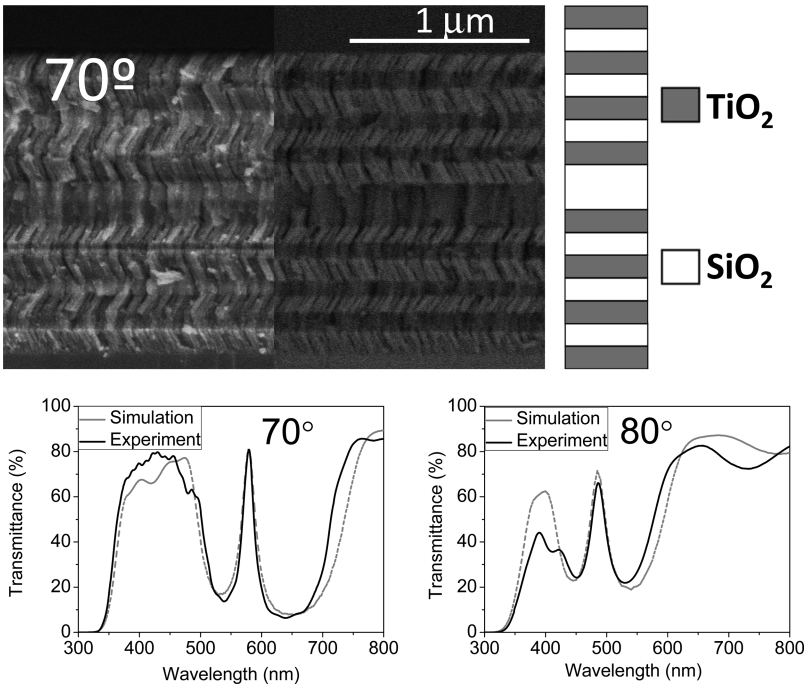

Figure 2. (top) Cross-section SEM micrograph (bright and dark fields) of a cleaved microcavity prepared by evaporation at a 70° zenithal angle. The scheme shows the stacking order of the individual layers forming the microcavity. (Bottom) UV−vis transmission spectra of microcavities prepared at 70° (left) and 80° (right) zenithal angles. Simulated spectra are plotted for comparison.

ature,[5,13,14,17−19] the GLAD methodology is advantageous because it is compatible with any sensitive substrate (e.g., polymers) and does not require any oxidation step at high temperatures to make the stacked layers transparent. Moreover, the large contrast between the refractive index of the individual SiO_2 and TiO_2 layers of the GLAD microcavities (SiO_2 and TiO_2 GLAD layers have refractive indices of 1.22/1.20 and 1.70/1.55 when prepared at 70° and 80°, respectively[22,23]) and their high pore volume (i.e., approximately 49% and 60% for these two evaporation angles[22,23]) make these optical devices suitable for a wide range of optofluidic applications.

The optical behavior of the microcavity structure was checked by UV−vis transmission spectroscopy. Figure 2 (bottom) shows the measured and simulated transmission spectra obtained for microcavities prepared at 70° and 80° zenithal angles of evaporation. These spectra depict the typical behavior of planar optical microcavities which, for the 70° case, consist of a wide reflecting region extending from approximately 500 to 700 nm and a narrow and sharp resonant peak located at 579 nm and a width at half height of 18.5 nm (i.e., a *Q* factor, defined as the ratio of the resonance cavity frequency to the line width of the cavity mode, of 31, with an error bar estimated by the determination of the position of the maxima of ±1 nm). For the 80° microcavity, these spectral parameters are 486 and 23.7 nm (*Q* factor 20), respectively. In this latter case, the position and other spectral features of the transmission spectra are well reproduced for $\lambda > 450$ nm, but deviations are observed below this wavelength value. We attribute the decrease in the transmitted light in this spectral region, enhanced at high zenithal angles, to light dispersion effects at the void and oxide material nanostructures formed in these films.[5,28]

For the individual layers, Table 1 summarizes the thickness values determined experimentally by SEM and those estimated by the simulation of the spectral features. The refractive index values of SiO_2 and TiO_2 required to get a good fitting are also included in this table. Within a variation of 10%, the limit of accuracy estimated for the simulations, the calculated refractive indices are similar to the experimental values of *n* previously determined for GLAD thin films of these materials.[22,23] In comparison with the *n* values of compact films of these two oxides (i.e., around 1.45 and 2.40 for SiO_2 and TiO_2, respectively[29]), the low value of this parameter obtained for the GLAD thin films confirms their high porosity and, hence, the possibility of modifying *n* if the pores are filled with liquids. The porosity values of the individual layers of the Bragg microcavity determined by simulation are reported in Table 1.

Table 1. Characteristic Layer Parameters of Bragg Microcavities Prepared at α = 70° and 80°[a]

zenithal angle/layer	thickness (exptl; nm)	thickness (sim; nm)	*n* (sim)	*n* with water (sim)	porosity (%; sim)
70° TiO_2	94	88	1.69	1.83	49
70° SiO_2	88	81	1.23	1.39	49
70° SiO_2 defect	224	178	1.21	1.39	52
80° TiO_2	82	88	1.55	1.72	60
80° SiO_2	80	86	1.20	1.38	55
80° SiO_2 defect	168	180	1.20	1.38	55

[a]Thickness and refractive index values are derived from the SEM measurements (exp) and by simulation of the transmission spectra (sim). Data are provided for the "as prepared" microcavities and for the microcavities integrated in an optofluidic device with water circulating through it.

3.2. Optofluidic Response of Microcavities. To check whether the optical response of the GLAD microcavities changes when their pores are filled with a fluid, we flowed a series of liquids of different refraction indices through a microfluidic device integrating the Bragg porous structure.

dx.doi.org/10.1021/am401685r | ACS Appl. Mater. Interfaces 2013, 5, 6743−6750

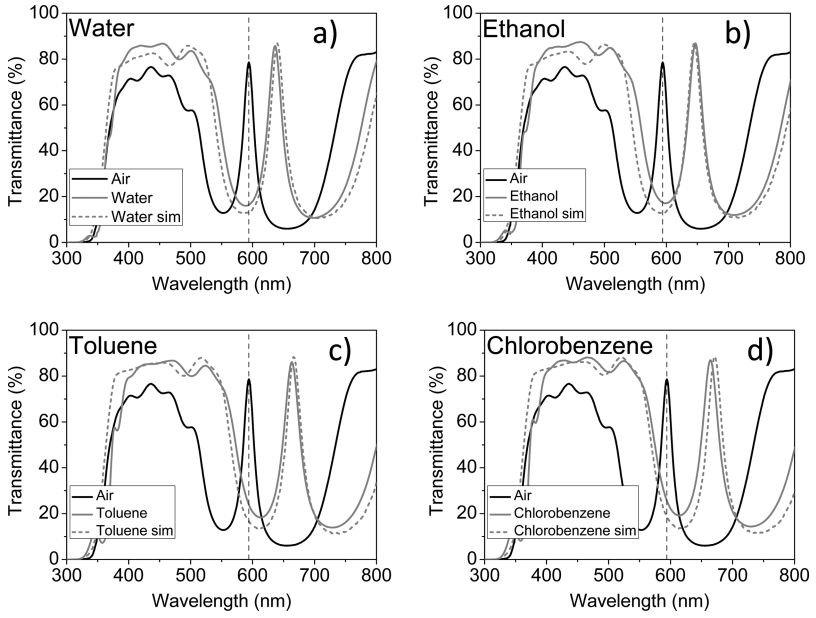

Figure 3. Experimental (full lines) and simulated (dashed lines) UV−vis transmission spectra of a microcavity device prepared at 70° before (black line) and after (gray lines) circulating different liquids through it: (a) water, (b) ethanol, (c) toluene, (d) chlorobenzene. The vertical lines indicate the position of the resonant peak in the microcavity without any liquid (i.e., with the pores filled with air).

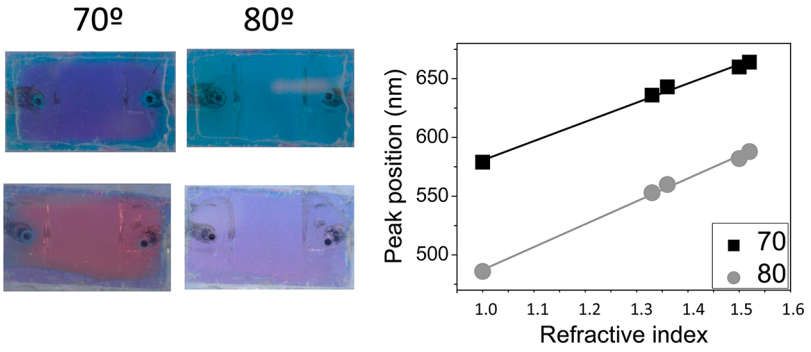

Figure 4. (Left) Images of 70° and 80° microfluidic devices empty (top) and filled with toluene (bottom). (Right) Plot of the position of the resonant peak in the UV−vis spectra of the 70° and 80° microcavity devices as a function of the refractive index of the infiltrated liquid.

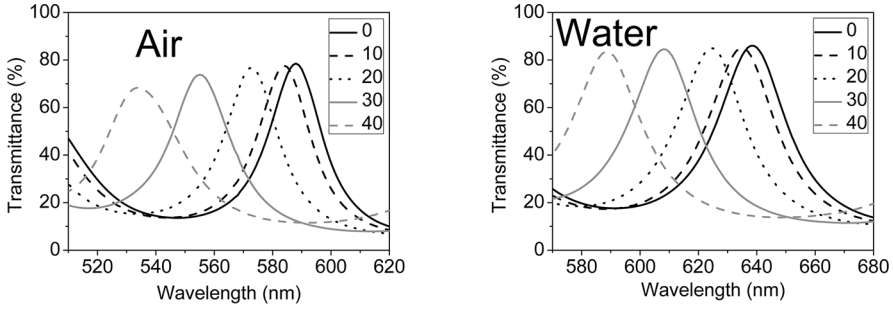

Figure 5. UV−vis transmission spectra for the indicated incident angles of light for an empty (left) and a water infiltrated (right) 70° microcavity structure.

Figure 3 shows the experimental and simulated UV−vis transmission spectra obtained for an empty 70° microcavity and after circulating through it liquids of different refractive indices (i.e., water (n = 1.330), ethanol (n = 1.361), toluene (n = 1.496), and chlorobenzene (n = 1.525)). An observed effect is a shift to longer wavelengths of both the transmission gap and the resonant peak. The magnitude of the shifts depends on the refractive index of the liquid and can be simulated by varying the effective refractive indices of each individual layer stacked in the microcavity. The values obtained for the case of water are gathered in Table 1, while the values deduced for the other liquids are reported in the Supporting Information (Table S2). Maximum error bars of approximately 0.02 units in n and ±10 nm for the thickness can be estimated for these calculations. The calculated refractive indices are higher than those of the empty (actually air-filled) layers as expected for a medium

dx.doi.org/10.1021/am401685r | ACS Appl. Mater. Interfaces 2013, 5, 6743−6750

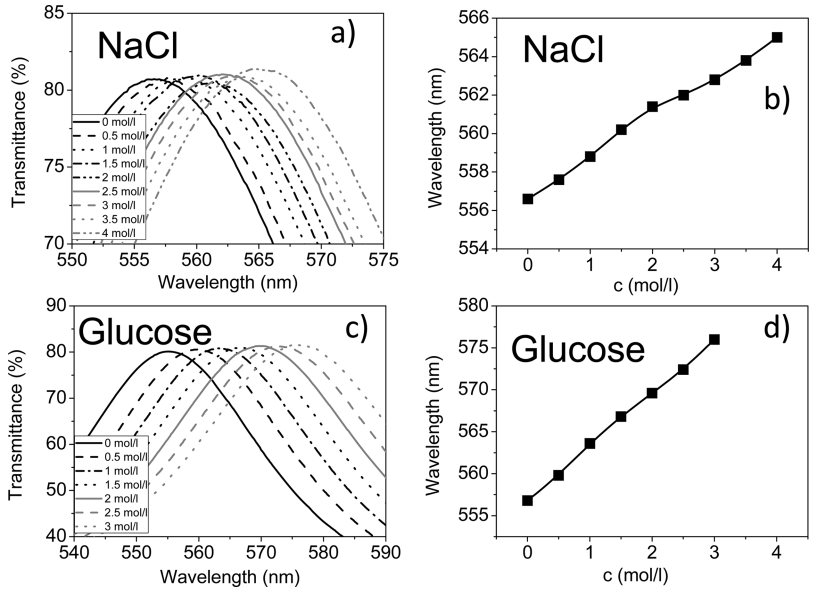

Figure 6. (Left) UV–vis transmission spectra for a 70° microcavity infiltrated with water and a series of NaCl (a) and glucose (c) solutions of the indicated concentrations. (Right) Plots of the shift in the position of the resonance peak as a function of NaCl (b) and glucose (d) concentrations. Note the different scales used for each plot.

consisting of a liquid filling the pores and voids of the individual films microstructure.

A similar behavior was observed for the microcavities prepared at 80°, with the additional effect that the transmission at low wavelengths recovered the level predicted by the theoretical simulation. This effect is attributed to the removal of light scattering effects by the liquids infiltrated through the otherwise empty micro- and mesopores (see Figure S3 in Supporting Information).

The overall optical changes induced by circulating liquids through the microcavity devices were so apparent that they could be observed with the bare eyes (c.f. Figure 4 (left)), thus opening the possibility of using them as visual tags.

From an analytical point of view, it is quite significant that the shift in the position of the resonant peak observed in Figures 3 and S3 can be directly related to the refractive index of the infiltrated liquid as reported in Figure 4 (right). This plot shows that the position of the maximum of the resonant peak varies almost linearly with the refractive index of the infiltrated liquid and supports that this kind of optofluidic device can be used to identify liquids of different refractive indices. A similar approach has been used to detect vapors of organic solvents by means of Bragg microcavities made of porous silicon layers of different porosities.[5,15,16]

A well-known behavior of compact Bragg microcavities is an angular dispersion in the position of the resonance peak when varying the incident angle of light.[27] As reported in Figure 5, porous microcavities behave in the same way either empty or filled with a liquid. This figure clearly shows that the resonant peak position shifts to shorter wavelengths when tilting the device with respect to the direction of light. Similar shifts were also observed for 80° microcavity structures (see Figure S4 in the Supporting Information). Within the angular variation monitored in this experiment, the resonance peak kept a similar height and width irrespective of the incident angle of light.

Similar angular variations were found for the porous microcavities filled with liquids (c.f., Figure 5 (right)), although the magnitude of the shift depended on the refraction index of the liquid. For example, turning by 40° the 70° microcavity resulted in a shift of 53 nm for the empty device and 48 and 54 nm for the systems filled with water and chlorobenzene, respectively. Similar effects could be appreciated for the microcavities prepared at 80° (see Figure S4 in the Supporting Information).

3.3. Optofluidic Analysis of Liquid Solutions by Means of GLAD Microcavities. The previous sections have dealt with the change in the optical response of porous microcavities when they are infiltrated with pure liquids. Due to the large difference in the refractive index of the porous TiO_2 and SiO_2 constituent layers, the microcavity device structures were very sensitive to small differences in the refractive index of the infiltrated liquids. Taking advantage of this enhanced sensitivity we propose to use these microcavities to determine the concentration of liquid solutions or the proportion of two liquids in a mixture. Some proofs of concept will be reported here to ascertain the feasibility of this analytical approach.

Figure 6 shows a series of UV–vis spectra in the region of the resonance peak for a 70° microcavity circulated with NaCl and glucose solutions with concentrations ranging from 0.5 to 4 mol/L and 0.5 to 3 mol/L, respectively. The spectra show that the peak position steadily varies with the solution concentration, a dependence that must be attributed to the different refraction index of the solutions.[30] Moreover, a representation of the peak position versus the solution concentrations yields in the two cases a practically linear dependence. These lines can be taken as calibration curves of glucose and NaCl concentrations for this particular device.

Monitoring the peak position requires a wavelength sensitive detector. Since intensity detectors are simpler, cheaper, and easier to operate, we explored an alternative way of measuring the solute concentration by looking to the angular variation of the peak position (cf. Figures 6 and S4) as a function of the solute concentration. The principle of the measuring procedure is reported in Figure 7, illustrated for the case of 70° microcavity, empty and filled with water. For a 0° incident angle of light, the resonance peak shifts to longer wavelengths

dx.doi.org/10.1021/am401685r | ACS Appl. Mater. Interfaces 2013, 5, 6743–6750

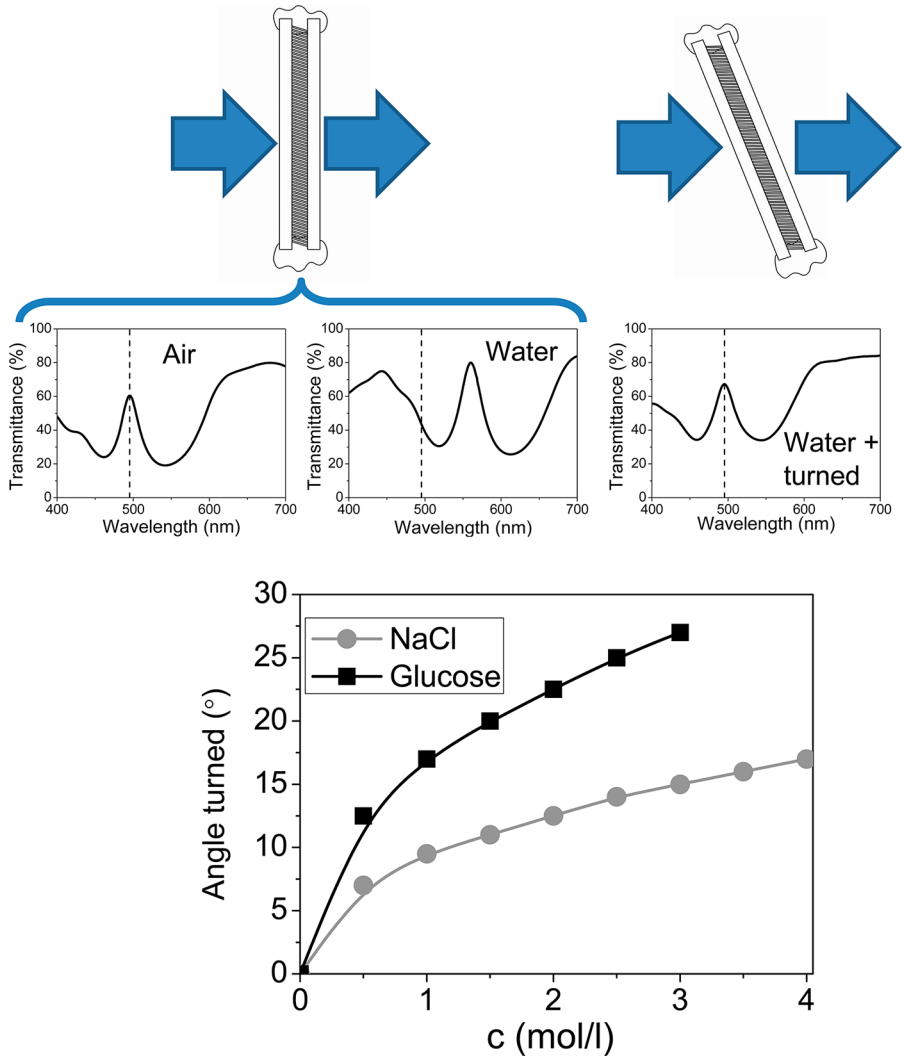

Figure 7. (Top) Scheme showing the variation of the position of the resonant peak when a microcavity is filled with water and the recovery of the initial wavelength position when the device is turned by a given angle. (Bottom) Correlation between the turned angles of the microcavity and the concentration of the NaCl and glucose solutions according to the procedure described in the scheme.

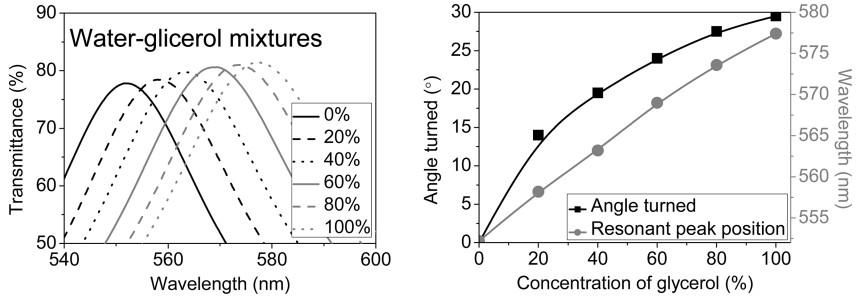

Figure 8. (left) UV−vis transmission spectra for a 70° microcavity infiltrated with mixtures of glycerol and water with different proportions of the two liquids. (Right) Plot of the shift in the position of the resonance peak and angle turned to restore its maximum intensity as a function of percentage of glycerol in the mixture.

when the device is infiltrated with water. This shift can be counterbalanced by turning the optofluidic device by an angle of 49° with respect to the light beam direction. For practical purposes, measurements of solution concentrations would be possible by using a single wavelength source (e.g., a LED) tuned to the resonance maximum of the microcavity, either empty or filled with water, an intensity detector, and a goniometer to measure the angular shift required to recover the maximum intensity of the transmitted light.

For the investigated NaCl and glucose solutions, Figure 7 shows the angular variations obtained as a function of the solution concentrations. Although the dependence is not linear, the depicted profiles follow well-defined calibration curves that can be used to determine the concentration of unknown solutions of these two substances.

dx.doi.org/10.1021/am401685r | ACS Appl. Mater. Interfaces 2013, 5, 6743−6750

Mixtures of liquids with different refraction indices can also be monitored by using GLAD microcavity devices, provided that they present sufficiently large differences of refractive indices. Figure 8 shows the results obtained for mixtures of glycerol (n = 1.473) and water (n = 1.330). The spectra and the plot in this figure are referred to the volume percentage of glycerol. It is apparent in this figure that the resonant peak shifts with the percentage of glycerol and that this shift follows well-defined dependences, when both representing the wavelength of the maximum of the resonant peak and the angle turned to recover its maximum intensity. These results clearly prove that an optofluidic device consisting of a porous microcavity prepared by GLAD can be used to determine the proportion of two liquids in a mixture, provided that their refraction indices differ sufficiently.

Besides these simple applications, we anticipate that this type of device will be useful for the continuous monitoring of liquids in microfluidic[31] or other analytical applications involving minute amounts of liquids (the pore volume of a microcavity device can be estimated in $\sim 7.5 \times 10^{-3}$ mm^3) or as cheap disposable systems for food control. As practical cases of this latter application field, Figures S5 and S6 of the Supporting Information report two examples showing how the developed microcavities can identify common beverages (different types of colas, isotonic drinks, etc.) or vegetable oils (e.g., olive or sunflower oils). Even if the viscosity of oils is rather high, its management through the microcavity structures is quite straightforward, which opens the way to the practical implementation of these devices for the analysis of a large variety of liquids. We must also stress that these devices could be manufactured in very small sizes due to the miniaturization possibilities of the GLAD techniques by combining their use with suitable masks to cover small portions of a substrate, while focusing the light beam for either excitation of detection. Direct depositing on microfluidic channels or previously made cavities is another alternative that should be explored in the future.

4. CONCLUSIONS

In this work, we have shown the electron-beam fabrication of GLAD planar porous microcavities consisting of successive layers of two oxides (SiO_2 and TiO_2) of different refractive indices. A strategy consisting of azimuthally turning the substrate from one layer to the next has been developed to minimize the light scattering effects usually observed for thick porous layers made by GLAD or other techniques. These microcavities have been very useful to determine the refraction index of liquids and solutions. The high transparency of the individual constituent layers and their high porosity has enabled their integration in the form of an optofluidc device where liquids fill and circulate through the void space of these structures. The simulation analysis of the changes observed in the transmission spectra of the microcavities after infiltration has proved that the position of the resonance peak depends on the refractive index of the liquid. This feature has been used systematically to determine the characteristics of the liquids by both measuring the position of the maximum and turning the photonic structure by a certain angle to restore the maximum intensity of the resonance peak at its initial wavelength. These two methods of detection have been successfully applied to determine the concentration of different solutions and mixtures of liquids.

The low volume of liquid required to induce these changes makes easy the implementation of the developed technology into complex microfluidic systems where it could provide a simple and reliable method of analysis. In addition, it could also be employed to develop switchable optofluidic components for switchable photonic applications.

■ ASSOCIATED CONTENT

Supporting Information

Additional details regarding the microstructure of Bragg microstructures prepared by evaporation at 80° and their behavior when infiltrated with different liquids and solutions. Practical case examples of the analysis of every-day live liquids. This material is available free of charge via the Internet at http://pubs.acs.org.

■ AUTHOR INFORMATION

Corresponding Author

*E-mail: arge@icmse.csic.es.

Notes

The authors declare no competing financial interest.

■ ACKNOWLEDGMENTS

We thank the Junta de Andalucía (Projects P09-CTS- 5189, TEP5283 and FQM-6900) and the Ministry of Science and Innovation (Projects, CONSOLIDER CSD2008-00023, MAT2010-21228, MAT2010-18447) for financial support.

■ REFERENCES

(1) Ge, J.; Yin, Y. *Angew. Chem., Int. Ed.* **2011**, 1492−1522.
(2) Holtz, J. H.; Asher, S. A. *Nature* **1997**, *389*, 829−832.
(3) Lee, Y. J.; Braun, P. V. *Adv. Mater.* **2003**, *15*, 563−566.
(4) Sharma, A. C.; Jana, T.; Kesavamoorthy, R.; Shi, L. J.; Virji, M. A.; Finegold, D. N.; Asher, S. A. *J. Am. Chem. Soc.* **2004**, *126*, 2971−2977.
(5) de Stefano, L.; Rendina, I.; Moretti, L.; Rossi, A. M. *Mater. Sci. Eng., B* **2003**, *100*, 271−274.
(6) Fan, X.; White, I. M. *Nat. Photonics* **2011**, *5*, 591−597.
(7) Wu, Z.; Lee, D.; Rubner, M. F.; Cohen, R. E. *Small* **2007**, *3*, 1445−1451.
(8) Colodrero, S.; Ocana, M.; Gonzalez-Elipe, A. R.; Miguez, H. *Langmuir* **2008**, *24*, 9135−9139.
(9) Choi, S. Y.; Mamak, M.; von Freymann, G.; Chopra, N.; Ozin, G. A. *Nano Lett.* **2006**, *6*, 2456−2461.
(10) Fuertes, M. C.; Lopez-Alcaraz, F. J.; Marchi, M. C.; Troiani, H. E.; Luca, V.; Miguez, H.; Soler-Illia, G. J. D. A. *Adv. Funct. Mater.* **2007**, *17*, 1247−1254.
(11) Lotsch, B. V.; Ozin, G. A. *ACS Nano* **2008**, *2*, 2065−2074.
(12) Guo, D.; Fan, L.; Wang, F.; Huang, S.; Zou, X. *J. Phys. Chem. C* **2008**, *112*, 17952−17956.
(13) Huanca, D. R.; Ramirez-Fernandez, F. J.; Salcedo, W. J. *Microelectron. Mater.* **2008**, *39*, 499−506.
(14) Torres-Costa, V.; Agulló Rueda, F.; Martín-Palma, R. J.; Martínez Duart, J. M. *Opt. Mater.* **2005**, *27*, 1084−1087.
(15) Gonzalez-Garcıa, L.; Lozano, G.; Barranco, A.; Mıguez, H.; Gonzalez-Elipe, A. R. *J. Mater. Chem.* **2010**, *20*, 6408−6412.
(16) Wang, Z.; Zhang, J.; Li, J.; Xie, J.; Li, Y.; Liang, S.; Tian, Z.; Li, Ch.; Wang, Z.; Wang, T.; Zhang, H.; Yang, B. *J. Mater. Chem.* **2011**, *21*, 1264−1266.
(17) Chan, S.; Li, Y.; Rothberg, L. J.; Miller, B. L.; Fauchet, P. M. *Mater. Sci. Eng., C* **2001**, *15*, 277−282.
(18) Palestrino, G.; Legros, R.; Agarwal, V.; Perez, E.; Gergely, C. *Sens. Actuators, B* **2008**, *135*, 27−34.
(19) Lu, X.; Mo, J.; Jiang, T.; Zhong, F.; Jia, Z.; Li, J.; Zhang, F. *Appl. Surf. Sci.* **2011**, *257*, 1906−1910.
(20) Jugessur, A. S.; Dou, J.; Aitchison, J. S. *J. Vac. Sci. Technol., B: Nanotechnol. Microelectron.: Mater., Process., Meas., Phenom.* **2010**, *28*, C6O8−C6O10.

(21) Gregg, S. J.; Sing, K. S. W. *Adsorption, Surface Area and Porosity*; Academic: London, 1982; p 25.
(22) Gonzalez-García, L.; Parra-Barranco, J.; Sanchez-Valencia, J. R.; Barranco, A.; Borras, A.; Gonzalez-Elipe, A. R.; Garcıa-Gutierrez, M. C.; Hernandez, J. J.; Rueda, D. R.; Ezquerra, T. A. *Nanotechnology* **2012**, *23*, 205701−205711.
(23) Gonzalez-García, L.; Parra-Barranco, J.; Sanchez-Valencia, J. R.; Ferrer, J.; Garcia-Gutierrez, M. C.; Barranco, A.; Gonzalez-Elipe, A. R. *Adv. Funct. Mater.* **2013**, *23*, 1655−1663.
(24) Brett, M. J.; Hawkeye, M. M. *Science* **2008**, *319*, 1192−1193.
(25) Harris, K. D.; Brett, M. J.; Smy, T. J.; Backhouse, Ch. *J. Electrochem. Soc.* **2000**, *147*, 2002−2006.
(26) Bezuidenhout, L. W.; Nazemifard, N.; Jemere, A. B.; Harrison, D. J.; Brett, M. J. *Lab Chip* **2011**, *11*, 1671−1678.
(27) Bass, M. *Handbook of Optics, Fundamentals, Techniques and Design*; Mc Graw-Hill Inc.: New York, 1995; Vol. *1*, Chapter 42: Optical properties of thin films and coatings, p 34.
(28) Gonzalez-Garcıa, L.; Gonzalez-Valls, I.; Lira-Cantu, M.; Barranco, A.; Gonzalez-Elipe, A. R. *Ener. Environ. Sci.* **2011**, *4*, 3426−3435.
(29) Lide, D. R. *CRC Handbook of Chemistry and Physics*, Internet Version; CRC Press: Boca Raton, FL, 2005; section 4, pp 151−154. http://www.hbcpnetbase.com.
(30) Yunus, W. N. N.; Rahman, A. A. *Appl. Opt.* **1988**, *27*, 3341−3343.
(31) Kuswandi, B.; Nuriman; Huskens, J.; Verboom, W. *Anal. Chim. Acta* **2007**, *601*, 141−155.